Journal of Applied Polymer Science

Near-Infrared Activation of Semi-Crystalline Shape Memory Polymer Nanocomposites

Duy M. Le, Michael A. Tycon, Christopher J. Fecko, Valerie S. Ashby
Department of Chemistry, University of North Carolina, Chapel Hill, North Carolina 27599
Correspondence to: V. S. Ashby (E-mail: ashby@email.unc.edu)

ABSTRACT: Recently, indirect activation of the shape memory effect has become an increasingly popular triggering modality for shape memory polymer biomaterials. Amongst the known methods for remote activation, near-infrared radiation (NIR) remains relatively unexplored, specifically for semicrystalline materials, which possess sharp thermal transitions. Herein, poly(ε-caprolactone) (PCL) networks were photo-polymerized from branched precursors doped with 150 nm surface modified gold nanoshells with a surface plasmon resonance of approximately 800 nm. The effect of nanoparticle loading on the thermal, mechanical, and shape memory properties of the PCL matrix were examined. The PCL nanocomposites exhibited excellent shape fixation and nearly quantitative shape memory recovery in response to low intensity NIR irradiation. Further, the heat dissipated by the irradiated nanocomposites to the surrounding medium was found to reach a maximum at biologically relevant temperatures. As such, this nanocomposite system represents a highly attractive candidate for many biomedical shape memory applications. © 2013 Wiley Periodicals, Inc. J. Appl. Polym. Sci. 000: 000–000, 2013

KEYWORDS: biomaterials; polyesters; composites

Received 25 March 2013; accepted 27 May 2013; Published online 27 July 2013
DOI: 10.1002/app.39604

INTRODUCTION

Shape memory polymers (SMPs) are a unique class of smart materials that change shape in a predetermined way when exposed to an external stimulus.[1] Since Lendlein and Langer first demonstrated their broad implications in biomaterials, SMPs have gained widespread interest for their uses as minimally invasive implants and self-deploying medical devices.[2–8] Thermally activated SMPs are thermoplastic elastomers or thermosets that are programmed by mechanically deforming the primary (permanent) shape of a polymer at temperatures which exceed its highest thermally reversible phase transition.[9] This transition temperature (T_{trans}) is closely associated with the polymer glass transition temperature (T_g) or melting temperature (T_m). Subsequently, the sample is cooled below T_{trans} while still under mechanical load. Retention of the secondary (temporary) shape is achieved through a sharp reduction in molecular mobility via crystallization or vitrification of the polymer. Primary shape recovery is then attained by heating the unconstrained network above T_{trans}. The resulting increase in chain mobility facilitates an entropically driven recovery of the original network shape.[10]

Recently, several novel approaches have been developed to enable the remote activation of the shape memory effect. These systems have expanded the breath of SMP applications by overcoming some of the limitations traditionally associated with direct thermal activation.[11] One such approach utilizes reversible photo-crosslinkable chemical moieties to facilitate the shape memory effect.[12–14] While, SMP systems based on photo-responsive chemical species are highly novel, these methods generally suffer from poor shape retention, slow shape recovery, and difficult or potentially harmful *in vivo* actuation. Polymer composites with magnetic fillers have also been investigated as a potential means of indirect activation. This platform utilizes the heat dissipated from the power loss of a magnetic filler to initiate the shape memory effect. Typical magnetic fillers include iron oxide particles, carbon nanotubes, and nickel-zinc ferrite particles.[15–19] Despite demonstrating significant improvements over photo-activated systems in terms of shape memory performance; magnetically driven SMP nanocomposites have been criticized for the high frequencies needed to induce complete shape recovery and are generally considered unsafe for biomedical applications.[20]

A promising triggering mechanism for remotely activated shape memory biomaterials is inductive localized heating using near-infrared (NIR) (700–1000 nm) absorbing nanoparticles. NIR absorbing fillers are highly attractive for safe and efficient transdermal SMP activation, as NIR absorbing chromophores are largely absent in most biological tissue.[21–25] In practice, NIR has been shown to have a tissue penetration depth up to

10 cm deep and has been utilized with excellent precision.[26] In particular, gold nanoparticles are ideal for remote SMP activation due to their demonstrated biocompatibility, highly tunable and biologically benign optical properties, and unparalleled light-to-heat conversion efficiency.[27] Moreover, the absorption cross-section at the surface plasmon resonance (SPR) wavelength is several orders of magnitude larger than conventional photo-absorbing dyes and are highly resistant to photo-bleaching.[28] As such, gold nanoparticles have been widely employed in numerous biomedical applications including the selective ablation of tumors, targeted drug delivery, and biological sensing.[29–32]

Recently, gold nanoparticles have also been exploited for remote SMP activation. Gold nanoparticles have been shown to be effective in remotely eliciting the shape memory effect for several SMP matrices including: poly(urethanes) and poly(β-amino esters).[33,34] These initial findings have demonstrated that gold nanoparticles can be used successfully to remotely initiate the shape memory effect in amorphous networks. However, there are by comparison, even fewer studies that have reported the use of gold nanoparticles in semicrystalline SMPs and to our knowledge no reports of photothermally induced semicrystalline shape memory materials in the NIR optical window.[11] Melting-temperature mediated SMPs intrinsically possess much more rapid and uniform shape memory transitions than their amorphous counterparts, and may be more attractive for high performance biological applications that require particularly fast and homogeneous transformations.[35–37]

We were interested in expanding upon these initial findings by establishing the potential of NIR absorbing gold nanoparticles in biodegradable semicrystalline SMP materials. Few studies have investigated the structure–property relationships between NIR absorbing fillers and semicrystalline polymers. As such, several key underlying factors need to be addressed including, the effect of nanoparticle incorporation on the degree of crystallinity (χ_c), T_m, the thermomechanical properties, and their broader implications for shape fixation (R_f), shape recovery (R_r), and shape recovery speed. Herein, we describe the synthesis of photo-crosslinkable poly(ε-caprolactone) (PCL) networks doped with surface modified 150 nm gold nanoshells with a SPR of approximately 800 nm. The effect of nanoparticle loading on the χ_c of the PCL matrix was examined by differential scanning calorimetry (DSC) while thermomechanical studies were studied by tensile analysis at temperatures above and below T_{trans}. The PCL nanocomposites showed exceptional R_f values and demonstrated sharp and nearly quantitative R_r values at low incident laser power intensities. Additionally, the heat dissipated from the PCL nanocomposites was shown to reach a maximum at biologically relevant temperatures. Examples of bulk shape memory transformations are provided in addition to the first example of NIR responsive shape memory polymer microarrays.

EXPERIMENTAL

Polymer Synthesis and Network Fabrication

The synthesis of star-shaped PCL prepolymers was previously described in the literature.[35] Briefly, prepolymers were synthesized by bulk ROP of ε-caprolactone using tin octanoate and glycerol ($<M_n>$ = 14,500 g mol^{-1}). The hydroxy-terminated oligo-PCL was refluxed with 2-isocyanatoethyl methacrylate and tin octanoate in anhydrous methylene chloride. PCL networks were prepared by adding a small aliquot of gold nanoshells dispersed in chloroform into the PCL trimethacrylate melt containing DEAP. The resulting mixture was cast into a Teflon mold and irradiated with 30 mW cm^{-2} UV light (365 nm) under N_2 atmosphere for 10 min. Gold nanoshells were purchased from Nanobio Spectra and were imaged using a FEI Helios 600 nanolab dual beam system. Absorbance spectra were obtained on a UV–vis spectrometer in the spectral range of 250–1000 nm.

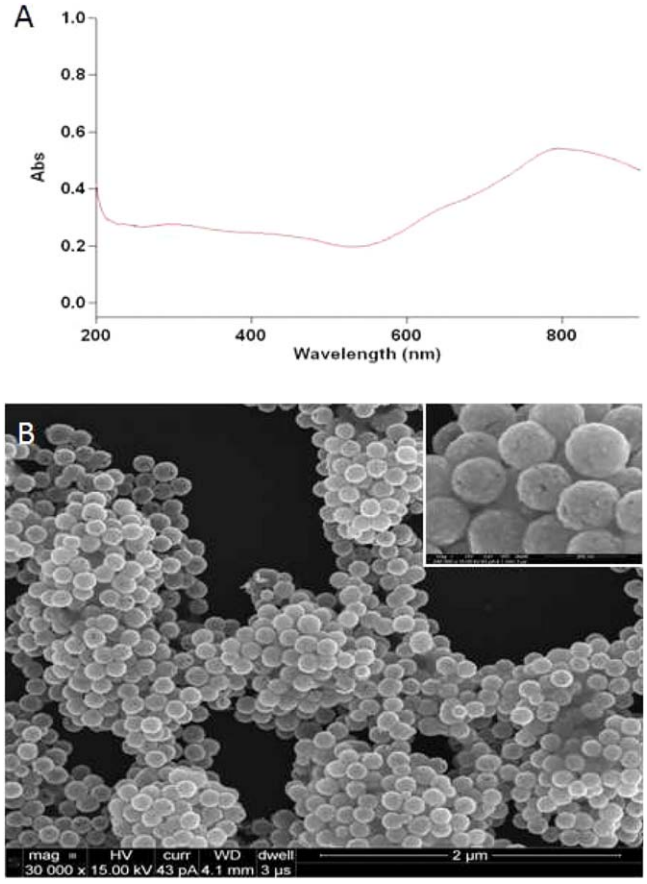

Figure 1. A: Absorbance spectrum of 150 nm gold nanoshells from 200 to 900 nm. B: SEM image taken at 30,000× magnification (Inset 240,000×), scale bar is 2 μm. [Color figure can be viewed in the online issue, which is available at wileyonlinelibrary.com.]

Thermal and Thermomechanical Characterization

Thermal characterization was performed on a TA instrument Q200 DSC, under nitrogen atmosphere from −20°C to 80°C with heating and cooling rates of 5°C min^{-1} and 10°C min^{-1}, respectively. Mechanical properties were analyzed on an Instron tensile analyzer using a constant strain rate of 10 mm min^{-1} at 22 and 50°C. The Young's modulus (E) was calculated using the initial linear portion of the stress/strain curve (0–5% strain).

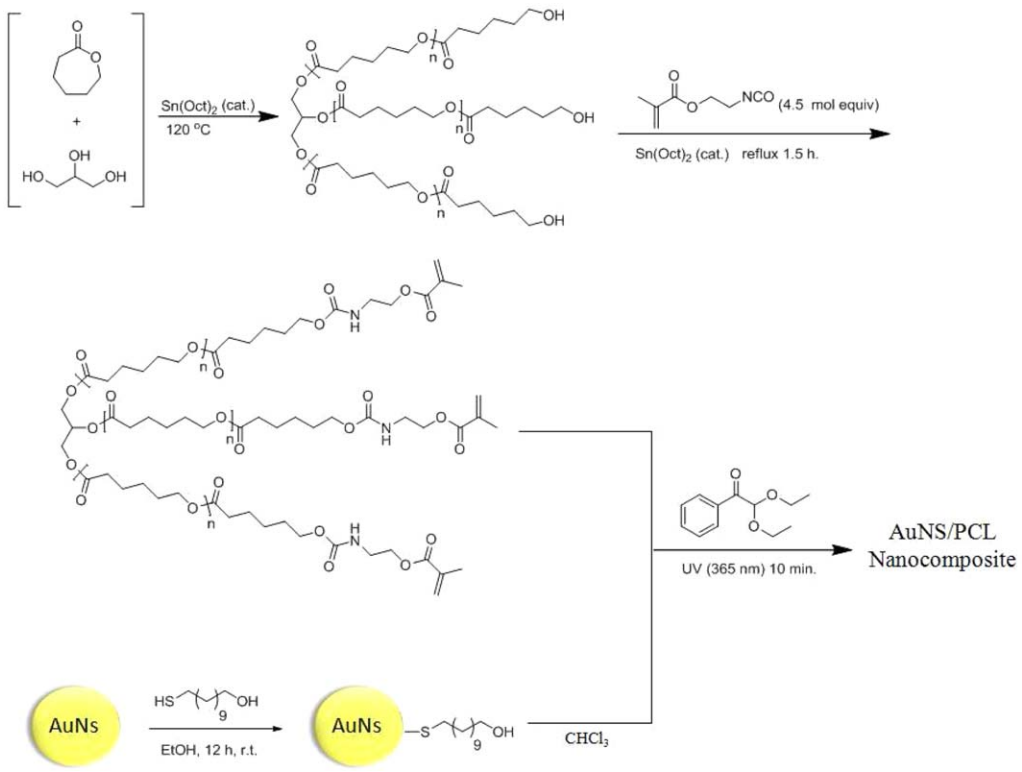

Figure 2. Synthesis of gold nanoshell/PCL nanocomposites. [Color figure can be viewed in the online issue, which is available at wileyonlinelibrary.com.]

Shape Memory Performance

Shape memory performance was analyzed by thermomechanical tensile analysis using an Instron analyzer. The equations for shape fixation (R_f) and shape recovery ratios (R_r) are as follows:

$$R_f = \frac{\varepsilon_u}{\varepsilon_m} \times 100 \quad (1)$$

$$R_r = \frac{\varepsilon_u - \varepsilon_p}{\varepsilon_m - \varepsilon_p} \times 100 \quad (2)$$

R_f is defined as the fixed strain after unloading (ε_u) to the total strain induced during deformation (ε_m). R_r is defined as the ratio of the difference between the strain after unloading (ε_u) and the permanent strain after recovery (ε_p) to the difference between the total strain induced during deformation (ε_m) and the permanent strain after recovery (ε_p).[30] PCL molds (1 mm × 37 mm × 3 mm) were heated above the T_m and extended to a strain of approximately 100%. The sample was then allowed to cool under load to room temperature. Subsequently, the load was removed and the fixed strain was recorded to determine the R_f. To measure R_r, a Coherent Chameleon Ti:sapphire laser was used to irradiate samples at 800 nm using varying power intensities at a constant beam diameter of 2 mm for a total irradiation time of 35 s.

Heat Dissipation Characterization

The temperature change during irradiation was determined as a function of sample mass to water volume. Polymer samples (30–35.2 mg) were placed in direct contact with a thermocouple probe (Physitemp Thermalert TH-5) and submerged in 2.0 mL of water, then irradiated for 120 s with temperature sampling every 10 s.

RESULTS AND DISCUSSION

Synthesis of Poly(ε-caprolactone) Nanocomposites

The synthesis of three-arm PCL methacrylate end-functionalized precursors and their corresponding SMP thermosets has previously been described in the literature, where they were shown to possess low cytotoxicity and excellent shape memory properties at physiological temperature.[35] In this study, 150 nm gold nanoshells with a SPR of 800 nm were incorporated into the PCL polymer matrix to facilitate NIR activation of the shape memory effect (Figure 1).

The nanoshells were surface modified to mitigate particle aggregation and improve compatibility with the polymer matrix.[38,39] The gold nanoshells were surface functionalizing with a monolayer of 1-undecanol by immersing the nanoparticles in a 2 m*M* ethanol solution of 11-mercapto-1-undecanol for 12 h (Figure 2). Following surface functionalization, the hydroxy-alkane thiol modified nanoparticles freely re-dispersed in chloroform after moderate sonication. A 100 μL aliquot of nanoshells dispersed in chloroform was added to the PCL precursor melt containing the photo-initiator DEAP. The mixture was cast into a Teflon mold and irradiated at 365 nm for 10 min under N_2 atmosphere.

Thermal Characterization

To determine the effect of gold nanoshell loading on the T_m, PCL networks were loaded with gold nanoshells at varying

Applied Polymer SCIENCE

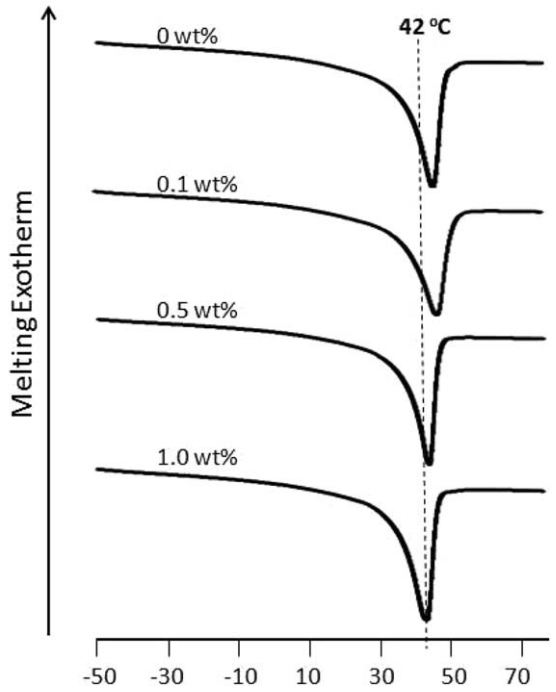

Figure 3. Effect of nanoshell loading on the T_m of the gold nanoshell/PCL nanocomposites.

weight fractions (0.0, 0.1, 0.5, 1.0 wt %) and analyzed by DSC in the temperature range of −60 to 80°C (Figure 3). Incorporation of nanoshells into the PCL matrix suppressed the formation of crystalline domains and resulted in a modest reduction in the T_m and χ_c with incremental nanoshell loading. The effect of nanoshell loading on T_m and χ_c is summarized in Table I.

All of the networks demonstrated sharp thermal transitions at biologically relevant temperatures. To achieve a near body temperature T_{trans}, a prepolymer chain length ($<M_n>$ = 14,500 g mol^{-1}) corresponding to a T_m of 45°C was chosen to compensate for the loss in crystallinity and the associated reduction in T_m incurred by nanoparticle incorporation. The highest nanoshell loading (1.0 wt %) resulted in a T_m of 42°C, which is consistent with clinical hyperthermic treatments. In all cases, the films exhibited sharp thermal transitions in the range of approximately 8°C, which were measured from the onset of melting to the peak of the melting exotherm. Buckley and coworkers demonstrated that the width of the phase transition is tightly correlated with shape memory recovery speed.[40,41] By comparison, glassy polymers generally possess thermal transitions many times broader than semicrystalline materials and therefore may be unsuitable for applications which require highly precise shape memory transformations.

Thermomechanical Characterization

Having shown the effect of nanoparticle weight fraction on T_m, the mechanical properties of dogbone films were then studied at 22 and 50°C by tensile analysis at a constant strain rate of 10 mm min^{-1}. The mechanical properties of neat PCL and nanocomposite films at 25 and 50°C are summarized in Table I. At 25°C, Young's modulus (E) decreased steadily with increasing nanoshell loading. Conversely, elongation at break (ε_R) increased with the addition of 0.1 wt % nanoshells and did not demonstrate any continued effect for larger nanoshell weight fractions. This loss in modulus and concurrent increase in extensibility is clearly due to the inhibitory effect of the gold nanoparticles on the formation of PCL crystallites which impart strength to the network. This phenomenon is supported by the reduction in T_m and χ_c of nanoshell loaded composite materials in comparison to pure PCL.

Table I. Thermal and Thermomechanical Characterization

			25°C		50°C	
Wt % AuNS	T_m (°C)[a]	χ_c (%)[a]	E (MPa)[c]	ε_R (%)[c]	E (MPa)[c]	ε_R (%)[c]
0.0	45	26	164	42	40	120
0.1	46	25	155	97	18	170
0.5	44	24	126	102	12	190
1.0	42	22	111	99	11	189

[a] Differential scanning calorimetry (DSC).
[b] χ_c: degree of crystallinity. Ratio of the heat of fusion (ΔH_m) to a perfect PCL crystallite (135 J g^{-1}).
[c] Tensile analysis.

At 50°C, all of the films are well above T_m and have been rendered completely amorphous. PCL films loaded with 0.1 and 0.5 wt % gold nanoshells exhibited a reduction in E and an increase in ε_R when compared to neat PCL samples. At 1 wt % nanoshell content, the mechanical properties reached a plateau and did not change with additional nanoshell incorporation. These findings are noteworthy, as the addition of rigid nanoparticles into SMP matrices is commonly used to improve recovery stress by increasing the rubbery modulus.[42,43] Yet in this system, we observe a marked decrease in E and increase in ε_R with increasing nanoparticle content. These results are similar to previous reports in the literature for surface modified nanoparticle/polymer nanocomposites at low weight fractions and can be attributed to two possible mechanisms.[44–46] The first is associated with the free volume created between network chains by nanoparticle surface ligands, resulting in a decrease in T_g. The second is related to the conformation of polymer chains neighboring surface modified nanoparticles, which have weak or neutral enthalpic interactions with the matrix. In addition to improved polymer-nanoparticle compatibility, surface functionalization can also reduce chain entanglement and minimize enthalpic interactions with the matrix, leaving entropic effects as the significant factor. Polymer chains near the surface of nanoparticles experience a decrease in conformational entropy, and consequently, a depletion zone develops around the nanoparticle due to an entropically driven repulsion of chains from the nanoparticle surface. The low chain density around the particle results in an increase in chain mobility and an associated reduction in T_g. It is possible that these effects are responsible for the losses in mechanical strength observed at temperatures above T_m when low weight fractions of surface modified gold nanoshells were incorporated into the PCL matrix.

Table II. Shape Fixation (R_f), Shape Recovery (R_r), and Heat Dissipation Characterization

Wt % AuNS	R_f (%)	R_{r1} (%)[a]	R_{r2} (%)[b]	R_{r3} (%)[c]	ΔT (°C)[d]	ΔT_f (°C)[e]
0.0	>99	1.4	1.3	1.4	6.9	28.6
0.5	97	2.0	37.4	92.7	12.9	34.6
1.0	97	4.0	48.4	97.9	16.9	38.5

[a] R_{r1}: 0.2 W cm^{-2}.
[b] R_{r2}: 0.6 W cm^{-2}.
[c] R_{r3}: 0.8 W cm^{-2}.
[d] ΔT: temperature differential.
[e] ΔT_f: final temperature. Thermal characterization was performed at 800 nm (0.8 W cm^{-2}) for 35 s.

Near-Infrared Radiation Initiated Shape Memory Performance

Shape memory performance was evaluated by determining R_f and R_r (Table II). PCL films (10 mm × 3 mm × 1 mm) were heated to well above the T_m and stretched to a maximum strain of approximately 100%. Subsequently, the samples were cooled to −78°C while still under mechanical load to induce crystallization. At 100% extension, pure PCL samples exhibited R_f values typically greater than 99%. In all cases, the addition of gold nanoshells resulted in a slight reduction in R_f (> 95%) due to an associated loss in crystallinity. The films were then irradiated with 800 nm NIR at varying power densities between 0.2 and 0.8 W cm^{-2} at a constant beam diameter of 15.69 mm for a total of 35 s irradiation time (Figure 4). The beam was sufficiently expanded to fully irradiate the film with uniform light intensity. Neat PCL films showed negligible recovery over the full range of beam intensities with only 1.4% recovery at the highest beam intensity. These results are consistent with the absorption spectrum of pure PCL. Shape recovery values for 0.1 wt % loaded nanocomposites were only marginally better at 5% recovery at the highest power density and consequently were not tested at lower spectral intensities. Films with 0.5 wt % nanoshell content showed similar recovery performance when irradiated at 0.2 W cm^{-2}. However, when the films were subjected to increasing power densities, a sharp nonlinear rise in R_r was observed with a final R_r value of 92.7% (0.8 W cm^{-2}). Similarly, films with 1.0 wt % nanoshell content only demonstrated an R_r value of 4.9% at 0.2 W cm^{-2}, which quickly rose with increasing laser power to a final R_r value of 97.9% (0.8 W cm^{-2}). Thus, we have shown that 0.5 and 1.0 wt % gold nanoshell/PCL composites possess excellent secondary shape retention and nearly quantitative shape recovery in response to low incident laser intensities. Moreover, shape recovery was very rapid and was achieved well within the total irradiation time.

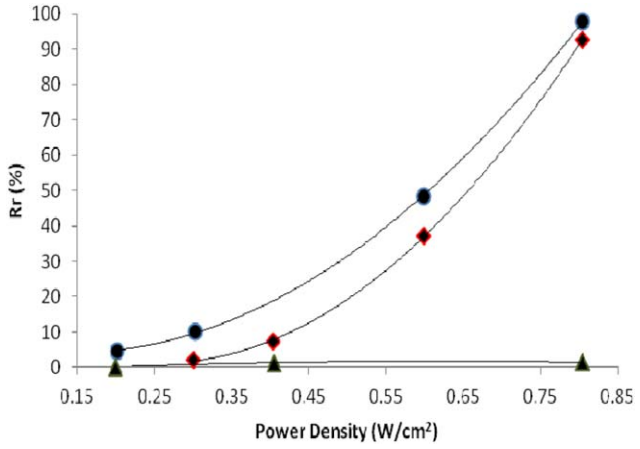

Figure 4. R_r measurements as a function of increasing incident NIR power density for 0 wt % (▲), 0.5 wt % (◆), and 1 wt % (●) gold nanoshell/PCL nanocomposites. [Color figure can be viewed in the online issue, which is available at wileyonlinelibrary.com.]

To demonstrate the bulk shape memory capabilities of the PCL nanocomposites, 1.0 wt % dogbone films were packaged into a rolled secondary shape and subsequently irradiated with NIR (800 nm, 0.8 W cm^{-2}) for 35 s to induce recovery (Figure 5). Upon NIR irradiation, the bulk films quickly unfurled and completely recovered their original unpackaged shape. Shape memory microarrays were also fabricated from 1.0 wt % films using a double replica imprint lithography technique previously described in the literature.[35] Films with a planar surface morphology were programmed into a temporary 3 μm × 5 μm channel microarray using poly(dimethylsiloxane) (PDMS) replica molds of a silicon master. These microarrays were also irradiated (800 nm, 0.8 W cm^{-2}) for a total of 35 s, and exhibited a complete return to their original planar surface topography.

These findings demonstrate that gold nanoshell/PCL composites exhibit sharp shape memory transformations in response to very low NIR incident power densities. Larger nanoparticle weight fractions modestly diminished R_f values and significantly increased R_r values, particularly at higher power densities. Moreover, the reduction in rubbery modulus observed in tensile analysis did not have an effect on recovery speed, as films with higher particle content generally recovered faster. This also represents the first example of a NIR activated SMP microarray and may be an effective and convenient platform for the dynamic investigation of cell–topography interactions and mechanotransductive events.[35,36,47–50]

Heat Dissipation Characterization

Heat dissipation is a key design parameter in remote shape memory biomaterials. Localized heating must be limited to the polymer matrix or remain below temperatures which cause cell damage while also supplying sufficient thermal energy to facilitate a complete shape transition. Having shown that gold nanoshell/PCL composites yield exceptional shape memory properties in response to low power densities, we next sought to demonstrate that the heat dissipated to the surrounding environment was biologically benign (Table II). To characterize the heat dissipation of the nanocomposites to the immediate environment, local temperature changes were recorded using a thermocouple placed in direct contact with the PCL nanocomposite films immersed in 2 mL of DI water. Films were irradiated with 800 nm light (0.8 W cm^{-2}) for a total of 180 s with temperature readings taken at 10 s intervals (Figure 6). All of the substrates showed a sharp increase in temperature during the first 40 s of irradiation before reaching a plateau. Pure PCL controls exhibited a 6.9°C increase in temperature resulting in a final temperature of 28.6°C. Substrates with 0.5 and

Applied Polymer SCIENCE

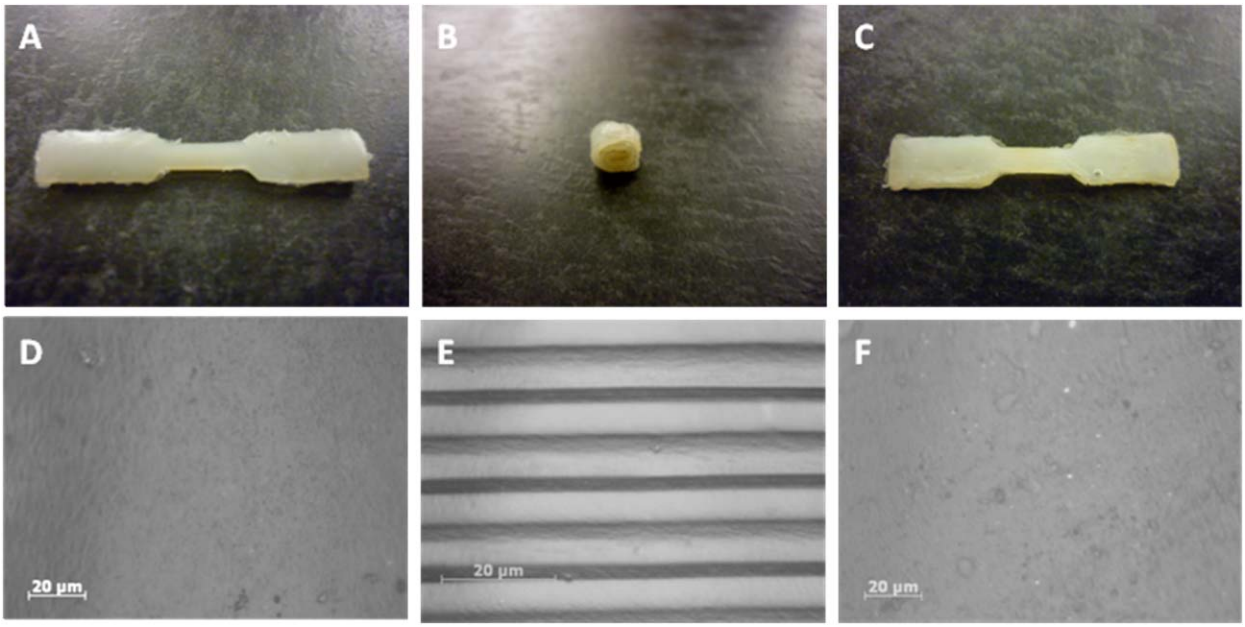

Figure 5. Images of a 1 wt % gold nanoshell/PCL nanocomposite in a (A) primary planar dogbone mold shape and (D) a permanent flat topography, (B) a secondary rolled up shape and (E) a secondary 3 μm × 5 μm channel topography, and (C) the recovered planar dogbone and (F) the recovered planar topography after irradiation with 800 nm (0.8 W cm^{-2}) for 35 s. [Color figure can be viewed in the online issue, which is available at wileyonlinelibrary.com.]

1.0% nanoshell contents exhibited 12.9 and 16.9°C increases in local temperature and final temperatures of 34.6 and 38.5°C, respectively. There is clearly a large temperature differential between the pure and nanoparticle loaded PCL samples pointing to the high light to heat conversion efficiency of the nanoshells. It is important to point out that the overall solution temperature remained below the T_m of the nanocomposites despite sufficient heat and irradiation time to induce a shape change. As a result of the low thermal conductivity of the PCL matrix, there is minimal heat dissipation to the surrounding medium. The temperature plateau represents an equilibrium reached between the internal film temperature and the heat dissipation to the surroundings. These results show that the heat dissipation of the gold nanoshells is capable of producing rapid and complete shape memory transformations yet remains below temperature, which may be potentially damaging to human tissue.

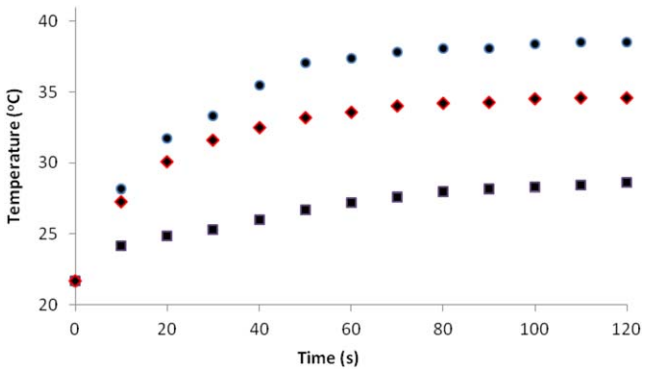

Figure 6. Heat dissipation as a function of time for gold nanoshell/PCL nanocomposites irradiated with 800 nm light (0.8 W cm^{-2}) at 0 wt % (■), 0.5 wt % (◆), and 1 wt % (●) nanoshell loading. [Color figure can be viewed in the online issue, which is available at wileyonlinelibrary.com.]

CONCLUSIONS

In summary, the fabrication and characterization of NIR activated gold nanoshell/PCL nanocomposites has been described. Incorporation of gold nanoshells into the PCL matrix marginally reduced the χ_c of the films and resulted in a decrease in T_m to within several degrees of body temperature. A loss in mechanical strength was observed in both the semicrystalline and rubbery regimes with increasing nanoparticle weight fraction. The gold/PCL nanocomposites demonstrated excellent R_f values which decreased only marginally with increasing nanoshell loading. Rapid and nearly quantitative R_r values were observed at both the macro-and microscale in response to low incident laser power densities at nanoshell concentrations of 0.5 and 1.0 wt %. Heat dissipation of the nanocomposite films was shown to rise quickly with NIR irradiation and taper off to a maximum near physiological temperature. We believe this new remote NIR activated SMP platform based on semicrystalline PCL materials and gold nanoshells may be a promising candidate for many biomedical applications, which require high performance shape memory properties.

ACKNOWLEDGMENTS

Funding for this work was provided from NSF DMR 0418499, SNSF PA00P3_124163, NIH 83008, and NSF PHY-1150017. The authors would like to thank Professor Kam Leong of Duke University for supplying the PDMS molds and Dr. Carrie Donnelly for her assistance with FIB imaging.

REFERENCES

1. Lendlein, A.; Kelch, S. *Angew. Chem. Int. Edit.* **2002**, *41*, 2034.
2. Lendlein, A.; Langer, R. *Science* **2002**, *31*, 1673.
3. Yakacki, C. M.; Shandas, R.; Lanning, C.; Rech, B.; Eckstein, A.; Gall, K. *Biomaterials* **2007**, *28*, 2255.
4. Liu, S. J.; Chiang, F. J.; Hsiao, C. Y.; Kau, Y. C.; Liu, K. S. *Ann. Biomed. Eng.* **2010**, *38*, 3185.
5. Chen, M. C.; Tsai, H. W.; Chang, W.; Lai, W. Y.; Mi, F. L.; Liu, C. T.; Wong, H. S.; Sung, H. W. *Biomacromolecules* **2007**, *8*, 2774.
6. Neuss, S.; Blomenkamp, I.; Stainforth, R.; Boltersdorf, D.; Jansen, M.; Butz, N.; Perez-Bouza, A.; Knüchel, R. *Biomaterials* **2009**, *30*, 1697.
7. Wischke, C.; Neffe, A. T.; Steuer, S.; Lendlein, A. *J. Control. Release* **2009**, *138*, 243.
8. Concepcion Serrano, M.; Carbajal, L.; Ameer, G. *A. Adv. Mater.* **2011**, *23*, 2211.
9. Mather, P. T.; Xiaofan, L.; Rousseau, I. A. *Annu. Rev. Mater. Res.* **2009**, *39*, 445.
10. Cao, F.; Jana, S. *Polymer* **2007**, *48*, 3790.
11. Zhang, H.; Xia, H.; Zhao, Y. *J. Mater. Chem.* **2012**, *22*, 845.
12. Kumpfer, J. R.; Rowan, S. J. *J. Am. Chem. Soc.* **2011**, *133*, 12866.
13. Wu, L.; Jin, C.; Sun, X. *Biomacromolecules* **2011**, *12*, 235.
14. Lendlein, A.; Jiang, H.; Jünger, O.; Langer, R. *Nature* **2005**, *434*, 879.
15. He, Z.; Satarkar, N.; Xie, T.; Cheng, Y. T.; Zach Hilt, J. *Adv. Mater.* **2011**, *23*, 3192.
16. Cai, Y.; Jiang, J.-S.; Zheng, B.; Xie, M.-R. *J. Appl. Polym. Sci.* **2013**, *127*, 49.
17. Schmidt, A. M. *Macromol. Rapid Commun.* **2006**, *27*, 1168.
18. Buckley, P. R.; McKinley, G. H.; Wilson, T. S.; Small, W.; Benett, W. J.; Bearinger, J. P.; McElfresh, M. W.; Maitland, D. J. *IEEE Trans. Biomed. Eng.* **2006**, *53*, 2075.
19. Mohr, R.; Kratz, K.; Weigel, T.; Lucka-Gabor, M.; Moneke, M.; Lendlein, A. *Proc. Natl. Acad. Sci. USA* **2006**, *103*, 3540.
20. Mather, P. T.; Luo, X.; Rousseau, I. *A. Annu. Rev. Mater. Res.* **2009**, *39*, 445.
21. Jain, P. K.; Huang, X.; El-Sayed, I. H. *Acc. Chem. Res.* **2008**, *41*, 1578.
22. Bardhan, R.; Lal, S.; Joshi, A.; Halas, N. *J. Acc. Chem. Res.* **2011**, *44*, 936.
23. Hirsch, L. R.; Stafford, R. J.; Bankson, J. A.; Sershen, S. R.; Rivera, B.; Price, R. E.; Hazle, J. D.; Halas, N. J.; West, J. L. *Proc. Natl. Acad. Sci. USA* **2003**, *100*, 13549.
24. Bardhan, R.; Chen, W.; Bartels, M.; Perez-Torres, C.; Botero, M. F.; McAninch, R. W.; Contreras, A.; Schiff, R.; Pautler, R. G.; Halas, N. J.; Joshi, A. *Nano Lett.* **2010**, *10*, 4920.
25. Huschka, R.; Zuloaga, J.; Knight, M. W.; Brown, L. V.; Nordlander, P.; Halas, N. J. *J. Am. Chem. Soc.* **2011**, *133*, 12247.
26. Fomina, N.; McFearin, C. L.; Sermsakdi, M.; Morachis, J. M.; Almutairi, A. *Macromolecules* **2011**, *44*, 8590.
27. Jain, P. K.; Lee, K. S.; El-Sayed, I. H.; El-Sayed, M. A. *J. Phys. Chem. B* **2006**, *110*, 7238.
28. Kennedy, L. C.; Bickford, L. R.; Lewinsky, N. A.; Coughlin, A. J.; Hu, Y.; Day, E. S.; West, J. L.; Drezek, R. A. *Small* **2010**, *7*, 169.
29. Chen, J.; Glaus, C.; Laforest, R.; Zhang, Q.; Yang, M.; Gidding, M.; Welch, M. J.; Xia, Y. *Small* **2010**, *6*, 811.
30. Pornpattananangkul, D.; Zhang, L.; Olson, S.; Aryal, S.; Obonyo, M.; Vecchio, K.; Huang, C.-M.; Zhang, L. *J. Am. Chem. Soc.* **2011**, *133*, 4132.
31. Marega, R.; Karmani, L.; Flamant, L.; Nageswaran, P. G.; Valembois, V.; Masereel, B.; Feron, O.; Borght, T. V.; Lucas, S.; Michiels, C.; Gallez, B.; Bonifazi, D. *J. Mater. Chem.* **2012**, *22*, 21305.
32. Wang, J.; Yao, H.-B.; He, D.; Zhang, C.-L.; Yu, S.-H. *ACS Appl. Mater. Interfaces* **2012**, *4*, 1963.
33. Hribar, K. C.; Metter, R. B.; Ifkovits, J. L.; Troxler, T.; Burdick, J. A. *Small* **2009**, *5*, 1830.
34. Xiao, Z.; Wu, Q.; Luo, S.; Zhang, C.; Baur, J.; Justice, R.; Liu, T. *Part. Part. Syst. Charact.*, to appear.
35. Le, D. M.; Kulangara, K.; Adler, A. F.; Leong, K. W.; Ashby, V. S. *Adv. Mater.* **2011**, *23*, 3278.
36. Brosnan, S. M.; Brown, A. H.; Ashby, V. S. *J. Am. Chem. Soc.* **2013**, *135*, 3067.
37. Wischke, C.; Lendlein, A. *Pharm. Res.* **2010**, *27*, 527.
38. Jordan, J.; Jacob, K. I.; Tannenbaum, R.; Sharaf, M. A.; Jasiuk, I. *Mater. Sci. Eng. A* **2005**, *393*, 1.
39. Thostenson, E. T.; Li, C.; Chou, T. W. *Compos. Sci. Technol.* **2005**, *65*, 491.
40. Buckley, C. P.; Prisacariu, C.; Caraculacu, A. *Polymer* **2007**, *48*, 1388.
41. Rousseau, I. *A. Polym. Eng. Sci.* **2008**, *48*, 2075.
42. Miaudet, P.; Derré, A.; Maugey, M.; Zakri, C.; Piccione, P. M.; Inoubli, R.; Poulin, P. *Science* **2007**, *318*, 1294.
43. Gall, K.; Dunn, M. L.; Liu, Y.; Stefanic, G.; Balzar, D. *Appl. Phys. Lett.* **2004**, *85*, 290.
44. Lee, J. Y.; Zhang, Q.; Emrick, T.; Crosby, A. *J. Macromolecules* **2006**, *39*, 7392.
45. Stafford, C. M., Harrison, C.; Beers, K. L.; Karim, A.; Amis, E. J.; Vanlandingham, M. R.; Kim, H. C.; Volksen, W.; Miller, R. D.; Simonyi, E. E. *Nat. Mater.* **2004**, *3*, 545.
46. Lee, J. Y.; Su, K. E.; Chan, E. P.; Zhang, Q.; Emrick, T.; Crosby, A. *J. Macromolecules* **2007**, *49*, 7755.
47. Kloxin, A. M.; Benton, J. A.; Anseth, K. S. *Biomaterials* **2010**, *31*, 1–8.
48. Lam, M. T.; Clem, W. C.; Takayama, S. *Biomaterials* **2008**, *29*, 1705.
49. Davis, K. A.; Burke, K. A.; Mather, P. T.; Henderson, J. H. *Biomaterials* **2011**, *32*, 2285.
50. Guvendiren, M.; Burdick, J. A. *Adv. Healthcare Mater.* **2013**, *2*, 155.